

[N I] 10400/10410 Å Lines as Possible Disk Wind Tracers in a Young Intermediate-Mass Star

HARUKI KATOH,^{1,2} CHIKAKO YASUI,³ YUJI IKEDA,^{4,2} NAOTO KOBAYASHI,^{5,6,2} NORIYUKI MATSUNAGA,^{7,2} SOHEI KONDO,^{5,2} HIROAKI SAMESHIMA,^{6,2} SATOSHI HAMANO,^{3,2} MISAKI MIZUMOTO,⁸ HIDEYO KAWAKITA,^{2,1} KEI FUKUE,^{2,9} SHOGO OTSUBO,² AND KEIICHI TAKENAKA^{2,1}

¹*Department of Physics, Graduate School of Science, Kyoto Sangyo University, Motoyama, Kamigamo, Kita-Ku, Kyoto, 603-8555, Japan*

²*Laboratory of Infrared High-resolution spectroscopy (LIH), Koyama Astronomical Observatory, Kyoto Sangyo University, Motoyama, Kamigamo, Kita-ku, Kyoto 603-8555, Japan*

³*National Astronomical Observatory of Japan, 2-21-1 Osawa, Mitaka, Tokyo 181-8588, Japan*

⁴*Photocoding, 460-102 Iwakura-Nakamachi, Sakyo-ku, Kyoto 606-0025, Japan*

⁵*Kiso Observatory, Institute of Astronomy, School of Science, The University of Tokyo, 10762-30 Mitake, Kiso-machi, Kiso-gun, Nagano 397-0101, Japan*

⁶*Institute of Astronomy, The University of Tokyo, 2-21-1 Osawa, Mitaka, Tokyo 181-0015, Japan*

⁷*Department of Astronomy, Graduate School of Science, University of Tokyo, Bunkyo-ku, Tokyo 113-0033, Japan*

⁸*Science Education Research Unit, University of Teacher Education Fukuoka, 1-1 Akama-bunkyo-machi, Munakata, Fukuoka 811-4192, Japan*

⁹*Education Center for Medicine and Nursing, Shiga University of Medical Science, Seta Tsukinowa-cho, Otsu, Shiga, 520-2192, Japan*

(Received 2022 July 23; Revised 2024 February 6; Accepted 2024 February 9)

ABSTRACT

In this study, we performed high-resolution near-infrared (NIR) spectroscopy ($R = 28,000$; $\lambda = 0.90\text{--}1.35\ \mu\text{m}$) with a high signal-to-noise ratio on HD 200775, a very young (~ 0.1 Myr old) and massive intermediate-mass star (a binary star with a mass of about $10 M_{\odot}$ each) with a protoplanetary disk. The obtained spectra show eight forbidden lines of three elements: two of [S II] (10289 and 10323 Å), two of [N I] (10400 and 10410 Å), and four of [Fe II] (12570, 12946, 12981, and 13209 Å). This is the first time that the [N I] lines are detected in a young stellar object with a doublet deblended. Gaussian fitting of the spectra indicates that all line profiles have low-velocity components and exhibit blueshifted features, suggesting that all lines originate from the disk winds (magnetohydrodynamic disk wind and/or photoevaporative wind). Based on the fit, the [N I] and [Fe II] lines are categorized into narrow components, while the [S II] lines are at the boundary between broad and narrow components. These forbidden lines are suggested to be very promising disk wind tracers among the existing ones because they are in the NIR-wavelength range, which can be observed from early stages with high sensitivities. Among these lines, [N I] lines would be a rather powerful probe for deriving the basic physical parameters of disk wind gases. However, the study of these lines herein is limited to one object; thus, further studies are needed to examine their properties.

Keywords: Protoplanetary disks (1300); Stellar winds (1636); Star formation (1569); Herbig Ae/Be stars (723); T Tauri stars (1681); Pre-main sequence stars (1290); Near infrared astronomy (1093); High resolution spectroscopy (2096)

1. INTRODUCTION

Protoplanetary disks are disks of gas and dust surrounding a young star that are formed when the star is born in a molecular cloud and then gradually disappear

as the central star evolves into a main-sequence star. Because planets are formed in the process of disk evolution/dispersal, understanding the mechanism of the process is essential to elucidate the planet formation process. Disk dispersal can be divided into two main processes: mass accretion (Shakura & Sunyaev 1973; Lynden-Bell & Pringle 1974), in which disk gas accretes to the central star, and disk dissipation, in which disk

gas is ejected into interstellar space. Mass accretion activities have been confirmed in many objects, mainly by the observation of hydrogen emission lines. Comparisons of the fluxes and line profiles with theoretical models have revealed the basic properties of mass accretion, such as the mass accretion rate and the geometric structure of the accretion, and enabled their quantitative derivation (Hartmann et al. 2016).

Disk winds, such as magnetohydrodynamic (MHD) disk winds (e.g., Suzuki & Inutsuka 2009) and photoevaporative disk winds (e.g., Hollenbach et al. 1994), are considered to be the dominant mechanisms of disk dissipation. Recently, an increasing number of atomic and molecular transitions with line profiles indicative of disk winds have been observed (e.g., Pascucci et al. 2023), including optical forbidden lines (e.g., [O I] 5577/6300 Å and [S II] 4068/4076 Å; Hartigan et al. 1995), near-infrared (NIR) CO and H₂ transitions (Bary et al. 2003), infrared forbidden lines (e.g., [Ne II] 12.8 μm; Pascucci & Sterzik 2009, Pascucci et al. 2020), and CO rotational lines at millimeter wavelengths (Trapman et al. 2022). Among them, forbidden lines with blueshifted emission features will be the focus of this paper.

The line profiles of forbidden lines often show multiple components, including high-velocity components (HVCs; $|V_c| \approx 50\text{--}300 \text{ km s}^{-1}$), originating from jets, and low-velocity components (LVCs) with a central velocity $|V_c| \leq 30 \text{ km s}^{-1}$, which originate from disk winds (e.g., Hartigan et al. 1995). Recent high-dispersion spectroscopic observations have revealed that LVCs often have two components: a narrow component (NC) with a velocity width in FWHM $\Delta V_{\text{FWHM}} \leq 40 \text{ km s}^{-1}$ and a broad component (BC) with $\Delta V_{\text{FWHM}} > 40 \text{ km s}^{-1}$, although they cannot be clearly distinguished because they partially overlap (Simon et al. 2016; Banzatti et al. 2019). The complex profiles of LVCs with both BCs and NCs are not fully explained by MHD or photoevaporative disk winds, and their origin remains under debate. The BC in [O I] lines is inferred to be launched from radii of $\lesssim 0.5 \text{ au}$, ruling out a photoevaporative wind and instead pointing to an origin in MHD disk winds (Simon et al. 2016). Meanwhile, the NC is launched at larger disk radii of $\gtrsim 1 \text{ au}$ (as inferred from the smaller line widths), and its origin remains contentious to date. For example, after correlating the BCs and NCs, Banzatti et al. (2019) concludes that the luminosities decrease as the inner disk is dissipated, suggesting that both components originate in the MHD disk wind. A spectroastrometric study (Whelan et al. 2021) also suggests that the NC traces MHD disk wind.

Models of the disk winds, including detailed heating and cooling mechanisms, have been published and compared with the observed profiles of the forbidden lines from the observations, while for the molecular tracers there is currently a lack of a suitable hydrodynamic wind model coupled with a chemical model and a dust evolution model, and the interpretation of the observations has not progressed (Pascucci et al. 2023; Ercolano & Pascucci 2017). [Ne II] 12.8 μm model line profiles were produced based on photoevaporative winds (e.g., Alexander 2008, Ercolano & Owen 2010) and appear to reproduce well the profiles obtained from observations (Pascucci et al. 2020). Model line profiles of optical forbidden lines have also been calculated, for example, in Weber et al. (2020), suggesting that the combination of MHD and optical evaporation winds can explain the BC and NC composite profiles.

In this paper, we explored disk wind tracers in the NIR-wavelength range because they are more sensitive than observations in the optical- and mid-IR- (MIR-) wavelength ranges, where the disk wind tracers identified so far are located. In general, young objects that are still embedded in molecular clouds are difficult to observe owing to large extinctions in the optical bands and thermal radiations from the telluric atmosphere in the MIR range. Herein, we focus on intermediate-mass stars ($\sim 2\text{--}10 M_{\odot}$), which are more massive than low-mass stars that have been the subject of previous observations. We investigated novel disk wind tracers in the NIR-wavelength region, where emission lines from young stars are easily detected with a high signal-to-noise ratio (S/N). For example, several theoretical models have indicated that the higher photoevaporation efficiency of intermediate-mass stars (e.g., Gorti et al. 2009; Komaki et al. 2021; Kunitomo et al. 2021) can explain why the disk lifetime of these stars is shorter than that of low-mass stars (Yasui et al. 2014; Ribas et al. 2014), and direct observation of intermediate-mass stars would be an important next step. As a first target, we selected HD 200775, which is a young stellar object (YSO) with a massive intermediate stellar mass. The disk of HD 200775 is directly imaged in MIR bands (Okamoto et al. 2009).

The rest of this paper is organized as follows. Section 2 summarizes the properties of the target, observation, and data reduction. Section 3 presents the obtained NIR spectra, identifies the forbidden lines, and discusses their properties. In Section 4, we categorize the line profiles of the forbidden lines, discuss their origins and the possibility of disk wind in protoplanetary disks around intermediate-mass stars, and use the NIR

forbidden lines detected in this study as new disk wind tracers. Finally, the paper concludes in Section 5.

2. TARGET, OBSERVATION, AND DATA REDUCTION

2.1. HD 200775

We selected HD 200775 as a target, which has the earliest spectral type among YSOs with confirmed protoplanetary disks from the Catalog of Circumstellar Disks¹. Optical spectroscopy has shown that the spectral type is B3 (e.g., Hernández et al. 2004). From Gaia Data Release 3 (Gaia Collaboration et al. 2021), its astrometric distance is estimated as 348_{-4}^{+5} pc. HD 200775 is a binary system based on the time variability of the H α emission line (Miroshnichenko et al. 1998). The primary and secondary masses are $10.7 \pm 2.5 M_{\odot}$ and $9.3 \pm 2.1 M_{\odot}$, respectively. The semimajor axis of the orbit is 5.4 au, assuming a distance of 350 pc (Monnier et al. 2006; Alecian et al. 2008). The object is estimated to be very young (~ 0.1 Myr) (Aleician et al. 2008), and the mass accretion rate (\dot{M}_{acc}) and mass-loss rate (\dot{M}_{loss}) are very high ($\dot{M}_{\text{acc}} = 10^{-4.2} M_{\odot} \text{ yr}^{-1}$ and $\dot{M}_{\text{loss}} = 10^{-6.55} M_{\odot} \text{ yr}^{-1}$) (Arun et al. 2019; Damiani et al. 1994).

Considering the possibility of disk wind in HD 200775, Okamoto et al. (2009) reported that the free-free emission detected by Fuente et al. (2001) may be generated from the photoevaporation region in this star (although Fuente et al. (2001) considered the emission as a stellar wind origin) because R_g calculated based on the stellar mass (73–146 au) agrees well with the hole size of the disk obtained from their direct imaging in MIR bands. From the imaging, the disk inclination angle is estimated as $i = 54^{\circ}.1 \pm 1^{\circ}.2$.

2.2. Observation

We obtained the spectra of HD 200775 using the NIR spectrograph, WINERED (Ikeda et al. 2022), which is attached to the Araki 1.3 m telescope at Koyama Astronomical Observatory, Kyoto Sangyo University, Japan (Yoshikawa et al. 2012). WINERED is a high-sensitivity and high-resolution spectrograph. It provides two resolution modes with spectral resolving powers R of 28,000 and 70,000, called the “WIDE” and “HIRES” modes, respectively, and is customized for short NIR bands at 0.9–1.35 μm . In the WIDE mode, which was used in this study, the entire wavelength range of 0.9–1.35 μm is covered simultaneously in a single exposure. WINERED has a 1.7 μm cutoff 2048 \times 2048 HAWAII-

2RG infrared array with a pixel scale of $0''.75 \text{ pixel}^{-1}$. We used a slit of $1''.65$ wide and $45''$ long. Observations were performed on 2015 July 20. The sky condition was photometric with a relative humidity of 60%–75% throughout the night. The seeing size was $3''$ – $4''$. To achieve an accurate sky subtraction, all the observations were made by nodding the target along the slits on two slit positions, “A” and “B,” with one exposure per position. The spectra of “B” (“A”) are used for the sky spectra of “A” (“B”). This method is called ABBA dithering. We took four exposures (two A positions and two B positions), and the exposure time per frame was 600 s, resulting in a total exposure time of 2400 s for the target. ρ Peg with a spectral-type A1V was selected as the telluric standard star. It was considered with ABBA nodding within 1 hr of target data acquisition. The exposure time for a single frame was set to 120 s, and four sets of data were obtained, resulting in a total exposure time of 480 s. Details of the observations are listed in Table 1.

2.3. Data Reduction

All data were reduced using a WINERED data-reduction pipeline (Hamano et al. 2024). This pipeline includes the standard procedures of echelle spectroscopy: bad pixel masking, sky subtraction, flat-fielding, scattered light subtraction, transformation of two-dimensional (2D) echelle image into a rectangular image with orthogonal space and wavelength axes, spectrum extraction, and continuum normalization. To extract the one-dimensional spectrum, the pixels corresponding to twice the FWHM ($7''$) were integrated in the spatial direction. The spectrum of HD 200775 was divided by the spectrum of the standard star (ρ Peg) in the procedure by Sameshima et al. (2018), which eliminates the photospheric features to correct the telluric absorption lines. For each echelle order, the spectra were normalized to 1.0 using the IRAF²/PyRAF continuum task. Finally, the spectra were corrected for heliocentric radial velocities (RVs) with 8.65 km s^{-1} , which varied within 0.01 km s^{-1} throughout the observations, using the IRAF/PyRAF rvcorrect task.

3. RESULTS

3.1. Detection of the Forbidden Lines

From the HD 200775 spectra obtained in Section 2.3, we focus on forbidden lines that can be disk wind trac-

¹ <https://www.circumstellardisks.org/index.php>

² IRAF is distributed by the National Optical Astronomy Observatories, which are operated by the Association of Universities for Research in Astronomy, Inc., under cooperative agreement with the National Science Foundation.

ers. Forbidden lines originate only from regions with electron densities lower than the critical electron density defined for each transition and have little or no self-absorption due to their low transition probabilities (Osterbrock & Ferland 2006). Therefore, forbidden lines can trace low-electron-density regions ($n_e \leq 10^8 \text{ cm}^{-3}$), where disk wind occurs. In addition, they can be very useful for accurately obtaining the velocity fields from their profiles.

In the obtained spectra, eight forbidden lines of three elements, [S II], [N I], and [Fe II], were detected at $S/N \geq 10$: two in [S II] (10289 and 10323 Å), two in [N I] (10400 and 10410 Å), and four in [Fe II] (12570, 12946, 12981, and 13209 Å). All forbidden lines are multiplets. When measuring the S/N of the emission lines, the noise levels were estimated from a region 3 Å away from both sides of the emission lines for 2 Å, a total of 4 Å from the long and short wavelength sides of the spectra. In the case where other lines were present in the 2 Å regions, the other continuum regions were used, where noise levels can be estimated in the same order as the emission lines. The S/Ns were calculated from the integrated intensity in the FWHM of the emission lines (S) and the measured noise level (σ_N) using the formula $\text{SNR} = S/\sqrt{\sigma_N^2 \times N_{\text{FWHM}}}$, where N_{FWHM} is the number of pixels included within the FWHM.

The properties of the detected lines are summarized in Table 2. The table lists the wavelength, Einstein A coefficient, and transition of each line obtained from NIST Atomic Spectra Database Lines Data³. All detected lines are shown as black lines in Figure 1 with respect to the stellar velocities. Based on several derivations of RV (see Bisyarina et al. 2015 for references), the measurements from stellar lines are expected to provide the most reliable estimates of the RV correction. In addition, as HD 200775 is a binary system, the systemic velocities derived from the data of two separated RVs over a long time period (years) are considered to be the most reliable. From this perspective, the derivations of Alecian et al. (2008) ($-7.9 \pm 0.9 \text{ km s}^{-1}$) and Bisyarina et al. (2015) ($-9.7 \pm 2.6 \text{ km s}^{-1}$) are considered as the most reliable velocities, and their weighted average, $-8.4 \pm 1.0 \text{ km s}^{-1}$, was adopted in the present analysis.

3.2. Derivation of Velocity Fields for the Detected Forbidden Lines

In this section, we determine the velocity fields for the forbidden lines detected in the HD 200775 spectra,

namely [S II], [N I], and [Fe II]. The spectra are fitted to a Gaussian profile with three parameters, the centroid velocity (V_c), the velocity width in FWHM ($\Delta V_{\text{FWHM}(\text{obs})}$), and the peak intensity relative to the continuum level (I_{peak}). For the [N I] 10400/10410 Å lines, because the emission lines are intrinsically doublets and the profiles are slightly asymmetric, each doublet was fitted to two components. Because each emission line requires three parameters for fitting, a naive fitting of the quadruple lines in [N I] requires 12 parameters. Assuming that collisional deexcitation is inefficient when forbidden lines are emitted, the intensity ratio of lines with a common upper level should be determined only by the ratio of their Einstein A coefficients. Among the four [N I] lines, the lines at 10401.004 and 10410.021 Å have common upper levels of $2s^2 2p^3 {}^2P_{3/2}^o$, while those at 10400.587 and 10410.439 Å have common levels of $2s^2 2p^3 {}^2P_{1/2}^o$. In addition, because the energy difference between the two upper levels is very small, these four lines are assumed to have the same regional origin, that is, the same V_c and $\Delta V_{\text{FWHM}(\text{obs})}$. Therefore, the original 12 fitting parameters can be reduced to four (one V_c value, one $\Delta V_{\text{FWHM}(\text{obs})}$ value, and two I_{peak} values).

In Figure 1, the blue and black lines are the obtained fitting profiles and the HD 200775 spectra, respectively. The intrinsic ΔV_{FWHM} was calculated from the instrumental profile correction on $\Delta V_{\text{FWHM}(\text{obs})}$ as $\sqrt{\Delta V_{\text{FWHM}(\text{obs})}^2 - \Delta V_{\text{FWHM}(\text{inst})}^2}$, where $\Delta V_{\text{FWHM}(\text{inst})}$ is the instrumental velocity width in FWHM. Because the spectral resolution of WINERED is almost constant ($R = 28,000$) over the entire wavelength range, the $\Delta V_{\text{FWHM}(\text{inst})}$ of all emission lines was assumed as 10.70 km s^{-1} .

Table 2 lists the three parameters, V_c , ΔV_{FWHM} , and I_{peak} , obtained from the fitting for each emission line. The uncertainties in V_c were sourced from those in the systemic velocity of HD 200775 ($\pm 1.0 \text{ km s}^{-1}$) and the observational errors. The V_c values obtained from all detected emission lines were $\gtrsim -5 \text{ km s}^{-1}$, indicating slightly blueshifted features. The [N I] and [Fe II] lines show narrow line widths with ΔV_{FWHM} of $\sim 15\text{--}20 \text{ km s}^{-1}$, whereas the [S II] lines show slightly wider line widths with ΔV_{FWHM} of $\sim 30\text{--}40 \text{ km s}^{-1}$.

4. DISCUSSION

4.1. Origin of the Forbidden Lines

Figure 2 categorizes the velocity properties of the forbidden lines into different velocity fields, HVC, LVC-BC, and LVC-NC (Simon et al. 2016; see Section 1). In this figure, the velocity properties of the detected forbidden

³ <https://www.nist.gov/pml/atomic-spectra-database>

lines ([S II], [N I], and [Fe II]) are plotted as circles, squares, and triangles, respectively. The quadruple [N I] lines are shown here as a single plot because they should have the same V_c and $V_{\text{FWHM(obs)}}$ values in the fitting (Section 3.2). The figure shows that $|V_c| \leq 30 \text{ km s}^{-1}$ for all emission lines and that all lines were classified as LVC, suggesting that they originated from disk wind. The line profiles [N I] and [Fe II] with narrow velocity widths ($\Delta V_{\text{FWHM}} \simeq 10\text{--}20 \text{ km s}^{-1}$) were categorized as LVC-NC whereas those of [S II] with slightly wider velocity widths ($\Delta V_{\text{FWHM}} \sim 30\text{--}40 \text{ km s}^{-1}$) were located at the boundary between LVC-BC and LVC-NC.

Note that line centroids for some lines (two [S II] lines and two [Fe II] lines) are within 1σ to the stellar velocity. This may be because the disk inclination angle of HD 200775 is relatively large ($i = 54.1 \pm 1.2$), which makes blueshifted features of line profiles less noticeable (Alexander 2008). Actually, disk wind tracers generally have small V_c values and some are estimated to be close to the stellar velocity or even redshifted (e.g., Banzatti et al. 2019 for the [O I] case). Nevertheless, the results that all forbidden lines detected here are estimated as blueshift suggest that they are all disk wind tracers. In particular, the result that all four [Fe II] lines, which are close to each other in energy level, show blueshifted features statistically supports that they are indeed blueshifted.

In previous studies, the same lines were also detected in YSOs (mainly in low-mass stars). The [S II], [N I], and [Fe II] lines with HVCs have been detected in ESO-H α 574 and Par-Lup 3-4 (Bacciotti et al. 2011; Giannini et al. 2013; Whelan et al. 2014). These lines have also been detected in other T Tauri stars, and all lines were classified in the literature as LVC ($-40 \lesssim v \lesssim 40 \text{ km s}^{-1}$), MVC (medium velocity component; $-100 \lesssim v \lesssim -40 \text{ km s}^{-1}$), or HVC ($v \lesssim -100 \text{ km s}^{-1}$). These lines with HVCs were also detected in a low-mass Herbig Halo object, HH34 (Nisini et al. 2016). The previous studies discussed these lines as jet tracers. The reason why these lines were detected as LVCs in HD 200775 but observed as various components in the low-mass T Tauri stars is unclear but may be explained by differences among the YSO masses. To resolve this problem, the [N I] line profiles must be comprehensively investigated through further WINERED observations or analyses of archival data. Moreover, to our knowledge, [N I] lines with a deblended doublet have not been detected in YSOs before. Notably, the two [N I] lines are further doublet (10400.587 and 10401.004 Å for [N I] 10400 Å, and 10410.021 and 10410.439 Å for [N I] 10410 Å), making quadruple lines in total, but they are not

resolved due to their intrinsic widths (see the following subsection).

4.2. Possible Origins Other than Stellar and Circumstellar Material Origin

The forbidden lines ([S II], [N I], and [Fe II]) detected in HD 200775 may not be intrinsic features of the object. Lowe et al. (1979), Luhman et al. (1998), and Walmsley et al. (2000) detected [S II] 10286/10320 Å, [N I] 10400/10410 Å, and [Fe II] 12570, 12946, 12981, 13209 Å forbidden lines in the bar structure in the Orion Nebula and photodissociation regions (PDRs). HD 200775 is located at the center of NGC 7023, a reflection nebula. From imaging observations of ultraviolet and optical bands, which have confirmed scattered light from the dust, the dust nebula extends to a radius of approximately $5'$ (e.g., Witt & Cottrell 1980; Witt et al. 1992). Furthermore, the nearby region of HD 200775 ($\leq 3'$) is surrounded by particularly dense nebular components. Imaging of the H $_2$ (1.18 and 1.21 μm) and CO emission lines in the NIR and radio wavelengths, respectively, has confirmed the presence of a bar structure, which is a PDR, approximately $1'$ away in the northwest and south directions from the central star (e.g., Sellgren et al. 1992; Lemaire et al. 1996; Gerin et al. 1998; Witt et al. 2006). Therefore, the forbidden lines detected here may not be intrinsic features of HD 200775 but contaminations from the foreground nebulae surrounding the objects. It could also be the influence of OH emission lines from the terrestrial atmospheric origin. To evaluate these possibilities, we investigated the spectra of regions somewhat away from the optical center of HD 200775 (hereafter, “reference regions”).

In this observation, a long slit of length $\sim 45''$ directed toward PA = 167° was used. Using 2D spectra reduced in the procedure of Section 2.3 but without sky subtraction and telluric corrections, we extracted the spectra of two regions approximately $10''$ and $30''$ from the optical center of HD 200775, with a width of $\sim 7''.5$. Because two reference regions can be set for each slit position A and B, there are four reference regions in total: $27''.0$ northwest, $8''.2$ northwest, $11''.1$ southeast, and $37''.8$ southeast of HD 200775. Figure 3 shows the spatial map of the reference regions around HD 200775. Because the focal plane array of WINERED is affected by latency and leaves afterimages for several hours when bright objects are taken for long periods (Ikeda et al. 2022), we selected the regions unaffected by afterimages as reference regions. The extracted spectra of the reference regions around the wavelengths of the [S II], [N I], and [Fe II] are shown with colored lines in Figure 4. The reference

spectra are relative fluxes to the HD200775 spectra normalized for the continuum level. For comparison, the HD 200775 spectra, which are reduced in the procedure in Section 2.3 (including sky subtraction and telluric correction), are also shown (black lines). The positions of OH emission lines of a terrestrial atmospheric origin (Oliva et al. 2013) are marked in the figure.

In the reference spectra, there are no positive features at wavelengths within 50 km s^{-1} of the forbidden lines detected in HD 200775 except around [S II] 10289 Å, [N I] 10400 Å, and [Fe II] 12946 Å. Therefore, all lines except these three forbidden lines cannot arise from contamination from the reference regions or OH emission lines. All features around the [S II] 10289 Å, [N I] 10400 Å, and [Fe II] 12946 Å lines seen in the reference spectra are consistent with the wavelengths of the OH emission lines and are of similar intensity to all reference spectra. Therefore, the positive features in the reference spectra are probably due to OH emission lines rather than the forbidden lines detected in HD 200775, which have somewhat different velocities. We cannot rule out that the forbidden lines with almost identical velocities and intensities are coincidentally observed in all four reference regions around HD 200775; however, in this case, the features are detected at wavelengths near the other forbidden lines of the same element because the three lines are multiplets. (For example, if [S II] is detected at 10289 Å, then [S II] will also be detected at 10323 Å. The same is true for [N I] 10410 Å for [N I] 10400 Å and [Fe II] 12570/129811/13209 Å for [Fe II] 12946 Å.) In summary, it is highly unlikely that the forbidden lines detected in HD 200775 represent contamination from surrounding regions. In addition, the velocities of the peaks of the forbidden lines in HD 200775 differ from those of the positive features seen in the reference spectra ($\gtrsim 20 \text{ km s}^{-1}$), so the forbidden lines (including the [S II] 10289 Å, [N I] 10400 Å, and [Fe II] 12946 Å forbidden lines) are unlikely to be OH emission lines.

4.3. Disk Winds around Intermediate-Mass Star

Blueshifted forbidden emission lines, such as [O I], [S II], and [Ne II], are known as disk wind tracers (e.g., Pascucci et al. 2023). Although the targets are mostly limited to low-mass stars, Acke et al. (2005) presented high spectral resolution optical spectra of 49 Herbig Ae/Be stars in a search for the [O I] 6300 Å line. The vast majority of stars in their sample showed emission lines with $\Delta V_{\text{FWHM}} < 100 \text{ km s}^{-1}$. Based on the profiles and the 5577/6300 [O I] ratio, Acke et al. (2005) suggested that the lines originated in the surface layers of the protoplanetary disks rather than in the disk winds as suggested for low-mass stars. The profiles might be

signatures of Keplerian rotation. The authors' interpretation was supported by the absence of the [S II] 6731 Å line in the emissions from their sample. The profiles of a small fraction of their sample, including HD 200775, show a high-velocity blue wing that cannot be explained by a Keplerian disk but is plausibly due to outflow. The emission lines of such objects, including HD 200775, usually show low-velocity double peaks on the blueshift and redshift sides of the stellar RV center. Because their profiles were consistent with the expected profiles of the emission-line regions on the disk surface, Acke et al. (2005) again interpreted the observed [O I] lines as disk emission features coming from the disk's atmosphere.

In the present paper, all detected forbidden lines from HD 200775 show LVCs with blueshifted features. Such features characterize the forbidden lines considered as disk wind tracers of low-mass stars. The morphology of the lines detected here differs from the [O I] lines (double-peaked LVCs and HVC) observed in HD 200775 by Acke et al. (2005). Meanwhile, Acke et al. (2005) detected no [S II] 6731 Å lines from HAeBes, which the authors interpreted as the absence of disk winds. In contrast, our observations detected [S II] 10289/10323 Å lines in HD 200775. These lines are transitions from a common upper level with [S II] 4068 Å, which is considered a disk wind tracer. Again, the results suggest disk wind in HD 200775 and can be traced through lines detected in our observations, although the origin of these lines must be investigated more precisely (e.g., by model fitting) in future work. HD 200775 is a massive intermediate-mass object, and the mass is located in the boundary region between intermediate- and high-mass stars. To our knowledge, we report the first indication of disk winds in such a massive intermediate-mass star from forbidden lines. The results suggest that disk winds are a universal process during disk evolution not only in low-mass stars but also in intermediate- and possibly high-mass stars.

The optically thick MHD disk winds are suggested to be effective in the early stages of the evolutionary process of disk dissipation (e.g., Suzuki & Inutsuka 2009). Theoretical studies (e.g., Hollenbach & Gorti 2009, Ercolano & Owen 2010) proposed that the inner winds in the early stages block energetic radiation from the central star and surrounding regions, preventing energetic radiation from reaching the disk and promoting photoevaporation, which is supported by the results of subsequent observations of [Ne II] forbidden lines (Pascucci et al. 2020). Photoevaporation then becomes effective in the middle stage of evolution, when the stellar and disk winds are weakening. The strength of stel-

lar and disk winds is quantified by the mass-loss rate (\dot{M}_{loss}), which correlates with the mass accretion rate to the central stars (\dot{M}_{acc}). In theoretical models, photoevaporation is only effective when $\dot{M}_{\text{acc}} \sim 10^{-7}$ to $\dot{M}_{\text{acc}} \sim 10^{-9} M_{\odot} \text{ yr}^{-1}$ (e.g., Wang & Goodman 2017; Nakatani et al. 2018; Picogna et al. 2019). Observationally, it has been proposed that photoevaporation begins to take effect when the mass accretion rate falls below $10^{-8} M_{\odot} \text{ yr}^{-1}$ (Pascucci et al. 2020). HD 200775 is very young (~ 0.1 Myr old; Alecian et al. 2008) and is estimated to have a high mass accretion rate ($\dot{M}_{\text{acc}} = 10^{-4.2} M_{\odot} \text{ yr}^{-1}$; Arun et al. 2019) and a high mass-loss rate ($\dot{M}_{\text{loss}} = 10^{-6.55} M_{\odot} \text{ yr}^{-1}$; Damiani et al. 1994). Therefore, it seems natural to assume that this is an MHD disk wind. However, the mass-loss rate due to photoevaporation is expected to be high for intermediate-mass stars of $10 M_{\odot}$, about 100 times higher than for low-mass stars of $1 M_{\odot}$ (Komaki et al. 2021).

Recently, Kunitomo et al. (2021) calculated the time evolution of the photoevaporation rates around young stars in the mass range covering intermediate-mass stars ($0.5\text{--}5 M_{\odot}$ stars). After considering the effect of stellar evolution on the evolution of protoplanetary disks, they suggested that far-UV emissions from the central star are sufficiently high for the generation of effective photoevaporative winds by a $5 M_{\odot}$ intermediate-mass star at a very young stage ($\lesssim 10^4$ yr). Therefore, photoevaporation is also a possible process in HD 200775, although HD 200775 is heavier than the upper mass considered in Kunitomo et al.’s model. However, the effects of the MHD disk wind and the stellar wind were excluded from this model and instead marked for future work.

4.4. NIR [N I] Lines as New Disk Wind Tracers

Forbidden lines, such as [O I] 5577/6300 Å and [S II] 4068/4076 Å in the optical band and [Ne II] 12.8 μm in the MIR wavelength region, are recognized as disk wind tracers (e.g., Pascucci et al. 2020). The forbidden lines detected here, [N I], [Fe II], and [S II], are all in the NIR range, which can be observed with high sensitivity. This is a significant advantage over [Ne II] 12.8 μm in the MIR-wavelength range as MIR wavelengths are not easily detected in ground-based observations, because they are largely affected by Earth’s atmosphere and the thermal ambient radiation. The lines in the NIR range also compare favorably with [O I] and [S II] lines in the optical range. In general, objects in the very young phase that are still embedded in molecular clouds are difficult to detect due to their large extinction in the optical bands. The extinction for [N I] 10400/10410 Å ($A_y/A_V \simeq 0.4$) is significantly smaller than the extinction for [S II] 4068/4076

Å ($A_g/A_V \simeq 1.2$) and [O I] 5577/6300 Å ($A_r/A_V \simeq 0.8$) (Wang & Chen 2019). Using recently developed high-sensitivity NIR high-dispersion spectrographs, high-S/N spectra can be obtained in a short time. Therefore, [N I], [Fe II], and [S II] lines are very useful for evaluating the presence or absence of disk winds and their physical parameters.

The [N I] lines also have an advantage in that they are relatively easy to detect. While [Ne II] 12.8 μm , [O I] 5577 Å, and [O I] 6300 Å are limited to the observed regions of electron density in the range $N_e = 10^2\text{--}10^6 \text{ cm}^{-3}$ (for $T_e = 2000\text{--}10,000$ K), $N_e = 10^6\text{--}10^7 \text{ cm}^{-3}$ (for $T_e = 4000\text{--}10,000$ K), and $N_e = 10^5\text{--}10^7 \text{ cm}^{-3}$ (for $T_e = 5000\text{--}8000$ K), respectively (Figure 5 of Pascucci et al. 2020), the [N I] 10400/10410 Å quadruplet lines are predicted to be the strongest among the different [N I] lines in the wide range of electron densities from $N_e = 10^2\text{--}10^{10} \text{ cm}^{-3}$ for $T_e = 5,000\text{--}10,000$ K according to the calculations by Kastner & Bhatia (1997). In addition, the total intensity of the four emission lines is predicted to be very sensitive to electron density. This intensity dependence over the wide electron density of the [N I] lines enables compensative studies of disk wind at any evolutionary stage. Actually, in Section 4.3 we suggested that disk winds could occur in HD 20075, which is still very young (~ 0.1 Myr old; Alecian et al. 2008) and has a very high mass accretion rate ($>10^{-5} M_{\odot} \text{ yr}^{-1}$; Arun et al. 2019). This indicates that the NIR lines, including the [N I] lines, are very sensitive to disk winds even at a very early stage. This is in contrast to [Ne II], which shows signs only at the late stage of disk evolution (Pascucci & Sterzik 2009). The NIR lines can serve as important tracers for capturing signs of disk winds in the early phases of protoplanetary disks, when material is still abundant.

The utility of [N I] 10400 and 10410 Å may be further enhanced by their quadruple line structure, which consists of two overlapping doublets (10400.587 and 10410.021, and 10401.004 and 10410.439 Å). The intensity ratio of the double lines formed by the separation of lower levels is determined solely by the ratio of the Einstein A coefficients, but the intensity ratio of the double lines formed by the separation of upper levels is known to depend strongly on the electron temperature and density (e.g., Osterbrock & Ferland 2006). Especially when the energy difference between upper levels is small, as is the case with [N I] 10400 and 10410, the intensity ratio is dominated by collisional deexcitation, making it very sensitive to electron density. Therefore, the emission lines of [N I] can potentially be a powerful probe for investigating the electron density of the disk wind. Furthermore, by using two pairs of double lines in

[N I] simultaneously, the accuracy of the electron density determination can be improved. In the future, we plan to develop photoionization models and advance spectroscopic diagnostics for [N I]. This will clarify the physical properties of the disk wind. In addition to the [N I] line, the [Fe II] and [S II] lines are multiplets and can be used to derive physical parameters in the same way as [N I].

5. CONCLUSION

In this study, we focused on intermediate-mass stars to search for new disk wind tracers (MHD disk wind and/or photoevaporative wind) in the NIR-wavelength range. We performed high-resolution NIR spectroscopy ($R = 28,000$; $\lambda = 0.91\text{--}1.33 \mu\text{m}$) on an intermediate-mass star, HD 200775, using WINERED. HD 200775 is a massive intermediate-mass star that has protoplanetary disks (a binary star with a mass of approximately $10 M_{\odot}$ each) and is very young (~ 0.1 Myr old). The main results are summarized as follows:

1. In the obtained HD 200775 spectra, eight forbidden lines that can be disk wind tracers of three elements were detected: two in [S II] (10289 and 10323 Å), two in [N I] (10400 and 10410 Å), and four in [Fe II] (12570, 12946, 12981, and 13209 Å). These are all multiple lines. Each of the [N I] lines consists of doublet lines, making a total of quadruple lines. This is the first time, to our knowledge, that [N I] lines were detected in YSO with a doublet deblended (10400 and 10410 Å).
2. We performed Gaussian fitting on the obtained spectra to estimate the central velocities and the velocity widths of the detected forbidden lines. In all the forbidden lines, the central velocity showed slightly blueshifted features of $\gtrsim -5 \text{ km s}^{-1}$. The FWHMs of [N I] and [Fe II] were narrow ($\sim 15\text{--}20 \text{ km s}^{-1}$), whereas those of [S II] were slightly wider ($\sim 30\text{--}40 \text{ km s}^{-1}$). All the forbidden lines were classified as LVCs, suggesting a disk wind origin. Based on the velocity fields of these emission lines, the [N I] and [Fe II] lines were categorized as LVC-NC, while the [S II] lines correspond to the boundary between LVC-NC and LVC-BC. These lines have been assumed as signatures of the jets of low-mass YSOs because they had been detected with various components (including HVCs) in such stars. The detection of all lines as LVCs in HD 200775 but as various components in low-mass T Tauri stars may be attributed to differences in the masses of the YSOs.
3. HD 200775 is located around the center of a reflection nebula, NGC 7023, which is associated with

PDRs, and the detected forbidden lines could be attributed to radiation from these regions. The detected lines can also be a result of contamination from OH emission lines during the observation. To verify these possibilities, we analyzed the spectra of the surrounding regions of HD 200775 without sky subtractions and telluric corrections. The reference spectra showed positive features around three of the eight forbidden lines detected in HD 200775, which were probably OH lines but were $\gtrsim 20 \text{ km s}^{-1}$ away from the forbidden lines in velocity. This suggests that the forbidden lines are not a result of contamination from the associated regions (i.e., the nebula and PDRs) or OH emission lines but are intrinsic features of the object.

4. The object in which the disk wind was observed herein, HD 200775, is an intermediate-mass star whose mass is in the boundary region with high-mass stars. This is the first indication of disk winds in such massive intermediate-mass stars from forbidden lines. This suggests that disk winds are a universal process in disk evolution not only for low-mass but also for intermediate-mass stars and possibly for high-mass stars. Recent observational results suggest that photoevaporative wind is ineffective in the early stages when the accretion rate is high because mass flows block the radiation from the central star, suggesting that the MHD disk wind is dominant, while the photoevaporative wind may be active in intermediate-mass stars because of the presence of strong far-UV in the early stages.
5. All the forbidden lines detected herein are in the NIR region; thus, they have a higher sensitivity for observing young stars from very early stages compared to previous disk wind tracers, such as [O I] and [S II] in the optical region and [Ne II] in the MIR region. Furthermore, all the forbidden lines are multiplets, and from their intensity ratio the physical parameters (temperature and density) of the gas can be determined by developing photoionization models. In particular, the [N I] lines, whose energy difference between the upper layers is very small, can be quite promising for the derivation with very high accuracy. This could reveal the physical properties of the disk wind gas. However, the discussion herein is limited to one object (HD 200775); thus, further investigation is needed to determine whether it can be applied to other YSOs.

ACKNOWLEDGMENTS

We thank Dr. Masanobu Kunitomo, Dr. Riouhei Nakatani, and Dr. Kei Tanaka for many useful comments. WINERED was developed by the University of Tokyo and the Laboratory of Infrared High-resolution Spectroscopy, Kyoto Sangyo University, under the financial support of KAKENHI (Nos. 16684001, 20340042, and 21840052) and the MEXT Supported Program for the Strategic Research Foundation at Private Universities (Nos. S0801061 and S1411028). This study was partly supported by Koyama Space Science Institute of Kyoto Sangyo University. KH is supported by JST SPRING, Grant Number JPMJSP2157.

Software: IRAF (Tody 1993), WINERED pipeline (Hamano et al. 2024).

REFERENCES

- Acke, B., van den Ancker, M. E., & Dullemond, C. P. 2005, *A&A*, 436, 209, doi: [10.1051/0004-6361:20042484](https://doi.org/10.1051/0004-6361:20042484)
- Alecian, E., Catala, C., Wade, G. A., et al. 2008, *MNRAS*, 385, 391, doi: [10.1111/j.1365-2966.2008.12842.x](https://doi.org/10.1111/j.1365-2966.2008.12842.x)
- Alexander, R. D. 2008, *MNRAS*, 391, L64, doi: [10.1111/j.1745-3933.2008.00556.x](https://doi.org/10.1111/j.1745-3933.2008.00556.x)
- Arun, R., Mathew, B., Manoj, P., et al. 2019, *AJ*, 157, 159, doi: [10.3847/1538-3881/ab0ca1](https://doi.org/10.3847/1538-3881/ab0ca1)
- Bacciotti, F., Whelan, E. T., Alcalá, J. M., et al. 2011, *ApJL*, 737, L26, doi: [10.1088/2041-8205/737/2/L26](https://doi.org/10.1088/2041-8205/737/2/L26)
- Banzatti, A., Pascucci, I., Edwards, S., et al. 2019, *ApJ*, 870, 76, doi: [10.3847/1538-4357/aaf1aa](https://doi.org/10.3847/1538-4357/aaf1aa)
- Bary, J. S., Weintraub, D. A., & Kastner, J. H. 2003, *ApJ*, 586, 1136, doi: [10.1086/367719](https://doi.org/10.1086/367719)
- Bisyarina, A. P., Sobolev, A. M., Gorda, S. Y., & Parfenov, S. Y. 2015, *Astrophysical Bulletin*, 70, 299, doi: [10.1134/S1990341315030074](https://doi.org/10.1134/S1990341315030074)
- Damiani, F., Micela, G., Sciortino, S., & Harnden, F. R., J. 1994, *ApJ*, 436, 807, doi: [10.1086/174957](https://doi.org/10.1086/174957)
- Ercolano, B., & Owen, J. E. 2010, *MNRAS*, 406, 1553, doi: [10.1111/j.1365-2966.2010.16798.x](https://doi.org/10.1111/j.1365-2966.2010.16798.x)
- Ercolano, B., & Pascucci, I. 2017, *Royal Society Open Science*, 4, 170114, doi: [10.1098/rsos.170114](https://doi.org/10.1098/rsos.170114)
- Fuente, A., Neri, R., Martín-Pintado, J., et al. 2001, *A&A*, 366, 873, doi: [10.1051/0004-6361:20000358](https://doi.org/10.1051/0004-6361:20000358)
- Gaia Collaboration, Brown, A. G. A., Vallenari, A., et al. 2021, *A&A*, 650, C3, doi: [10.1051/0004-6361/202039657e](https://doi.org/10.1051/0004-6361/202039657e)
- Gerin, M., Phillips, T. G., Keene, J., Betz, A. L., & Boreiko, R. T. 1998, *ApJ*, 500, 329, doi: [10.1086/305726](https://doi.org/10.1086/305726)
- Giannini, T., Nisini, B., Antonucci, S., et al. 2013, *ApJ*, 778, 71, doi: [10.1088/0004-637X/778/1/71](https://doi.org/10.1088/0004-637X/778/1/71)
- Gorti, U., Dullemond, C. P., & Hollenbach, D. 2009, *ApJ*, 705, 1237, doi: [10.1088/0004-637X/705/2/1237](https://doi.org/10.1088/0004-637X/705/2/1237)
- Hamano, S., Ikeda, Y., Otsubo, S., et al. 2024, *PASP*, 136, 014504, doi: [10.1088/1538-3873/ad1b38](https://doi.org/10.1088/1538-3873/ad1b38)
- Hartigan, P., Edwards, S., & Ghandour, L. 1995, *ApJ*, 452, 736, doi: [10.1086/176344](https://doi.org/10.1086/176344)
- Hartmann, L., Herczeg, G., & Calvet, N. 2016, *ARA&A*, 54, 135, doi: [10.1146/annurev-astro-081915-023347](https://doi.org/10.1146/annurev-astro-081915-023347)
- Hernández, J., Calvet, N., Briceño, C., Hartmann, L., & Berlind, P. 2004, *AJ*, 127, 1682, doi: [10.1086/381908](https://doi.org/10.1086/381908)
- Hollenbach, D., & Gorti, U. 2009, *ApJ*, 703, 1203, doi: [10.1088/0004-637X/703/2/1203](https://doi.org/10.1088/0004-637X/703/2/1203)
- Hollenbach, D., Johnstone, D., Lizano, S., & Shu, F. 1994, *ApJ*, 428, 654, doi: [10.1086/174276](https://doi.org/10.1086/174276)
- Ikeda, Y., Kondo, S., Otsubo, S., et al. 2022, *PASP*, 134, 015004, doi: [10.1088/1538-3873/ac1c5f](https://doi.org/10.1088/1538-3873/ac1c5f)
- Kastner, S. O., & Bhatia, A. K. 1997, *ApJS*, 109, 241, doi: [10.1086/312974](https://doi.org/10.1086/312974)
- Komaki, A., Nakatani, R., & Yoshida, N. 2021, *ApJ*, 910, 51, doi: [10.3847/1538-4357/abe2af](https://doi.org/10.3847/1538-4357/abe2af)
- Kunitomo, M., Ida, S., Takeuchi, T., et al. 2021, *ApJ*, 909, 109, doi: [10.3847/1538-4357/abdb2a](https://doi.org/10.3847/1538-4357/abdb2a)
- Lemaire, J. L., Field, D., Gerin, M., et al. 1996, *A&A*, 308, 895
- Lowe, R. P., Moorhead, J. M., & Wehlau, W. H. 1979, *ApJ*, 228, 191, doi: [10.1086/156835](https://doi.org/10.1086/156835)
- Luhman, K. L., Engelbracht, C. W., & Luhman, M. L. 1998, *ApJ*, 499, 799, doi: [10.1086/305682](https://doi.org/10.1086/305682)
- Lynden-Bell, D., & Pringle, J. E. 1974, *MNRAS*, 168, 603, doi: [10.1093/mnras/168.3.603](https://doi.org/10.1093/mnras/168.3.603)

- Miroshnichenko, A. S., Mulliss, C. L., Bjorkman, K. S., et al. 1998, *PASP*, 110, 883, doi: [10.1086/316208](https://doi.org/10.1086/316208)
- Monnier, J. D., Berger, J. P., Millan-Gabet, R., et al. 2006, *ApJ*, 647, 444, doi: [10.1086/505340](https://doi.org/10.1086/505340)
- Nakatani, R., Hosokawa, T., Yoshida, N., Nomura, H., & Kuiper, R. 2018, *ApJ*, 865, 75, doi: [10.3847/1538-4357/aad9fd](https://doi.org/10.3847/1538-4357/aad9fd)
- Nisini, B., Giannini, T., Antonucci, S., et al. 2016, *A&A*, 595, A76, doi: [10.1051/0004-6361/201628853](https://doi.org/10.1051/0004-6361/201628853)
- Okamoto, Y. K., Kataza, H., Honda, M., et al. 2009, *ApJ*, 706, 665, doi: [10.1088/0004-637X/706/1/665](https://doi.org/10.1088/0004-637X/706/1/665)
- Oliva, E., Origlia, L., Maiolino, R., et al. 2013, *A&A*, 555, A78, doi: [10.1051/0004-6361/201321366](https://doi.org/10.1051/0004-6361/201321366)
- Osterbrock, D. E., & Ferland, G. J. 2006, *Astrophysics of Gaseous Nebulae and Active Galactic Nuclei*
- Pascucci, I., Cabrit, S., Edwards, S., et al. 2023, in *Astronomical Society of the Pacific Conference Series*, Vol. 534, *Protostars and Planets VII*, ed. S. Inutsuka, Y. Aikawa, T. Muto, K. Tomida, & M. Tamura, 567, doi: [10.48550/arXiv.2203.10068](https://doi.org/10.48550/arXiv.2203.10068)
- Pascucci, I., & Sterzik, M. 2009, *ApJ*, 702, 724, doi: [10.1088/0004-637X/702/1/724](https://doi.org/10.1088/0004-637X/702/1/724)
- Pascucci, I., Banzatti, A., Gorti, U., et al. 2020, *ApJ*, 903, 78, doi: [10.3847/1538-4357/abba3c](https://doi.org/10.3847/1538-4357/abba3c)
- Picogna, G., Ercolano, B., Owen, J. E., & Weber, M. L. 2019, *MNRAS*, 487, 691, doi: [10.1093/mnras/stz1166](https://doi.org/10.1093/mnras/stz1166)
- Ribas, Á., Merín, B., Bouy, H., & Maud, L. T. 2014, *A&A*, 561, A54, doi: [10.1051/0004-6361/201322597](https://doi.org/10.1051/0004-6361/201322597)
- Sameshima, H., Matsunaga, N., Kobayashi, N., et al. 2018, *PASP*, 130, 074502, doi: [10.1088/1538-3873/aac1b4](https://doi.org/10.1088/1538-3873/aac1b4)
- Sellgren, K., Werner, M. W., & Dinerstein, H. L. 1992, *ApJ*, 400, 238, doi: [10.1086/171990](https://doi.org/10.1086/171990)
- Shakura, N. I., & Sunyaev, R. A. 1973, *A&A*, 24, 337
- Simon, M. N., Pascucci, I., Edwards, S., et al. 2016, *ApJ*, 831, 169, doi: [10.3847/0004-637X/831/2/169](https://doi.org/10.3847/0004-637X/831/2/169)
- Suzuki, T. K., & Inutsuka, S.-i. 2009, *ApJL*, 691, L49, doi: [10.1088/0004-637X/691/1/L49](https://doi.org/10.1088/0004-637X/691/1/L49)
- Tody, D. 1993, in *Astronomical Society of the Pacific Conference Series*, Vol. 52, *Astronomical Data Analysis Software and Systems II*, ed. R. J. Hanisch, R. J. V. Brissenden, & J. Barnes, 173
- Trapman, L., Tabone, B., Rosotti, G., & Zhang, K. 2022, *ApJ*, 926, 61, doi: [10.3847/1538-4357/ac3ed5](https://doi.org/10.3847/1538-4357/ac3ed5)
- Walmsley, C. M., Natta, A., Oliva, E., & Testi, L. 2000, *A&A*, 364, 301
- Wang, L., & Goodman, J. 2017, *ApJ*, 847, 11, doi: [10.3847/1538-4357/aa8726](https://doi.org/10.3847/1538-4357/aa8726)
- Wang, S., & Chen, X. 2019, *ApJ*, 877, 116, doi: [10.3847/1538-4357/ab1c61](https://doi.org/10.3847/1538-4357/ab1c61)
- Weber, M. L., Ercolano, B., Picogna, G., Hartmann, L., & Rodenkirch, P. J. 2020, *MNRAS*, 496, 223, doi: [10.1093/mnras/staa1549](https://doi.org/10.1093/mnras/staa1549)
- Whelan, E. T., Pascucci, I., Gorti, U., et al. 2021, *ApJ*, 913, 43, doi: [10.3847/1538-4357/abf55e](https://doi.org/10.3847/1538-4357/abf55e)
- Whelan, E. T., Bonito, R., Antonucci, S., et al. 2014, *A&A*, 565, A80, doi: [10.1051/0004-6361/201322037](https://doi.org/10.1051/0004-6361/201322037)
- Witt, A. N., & Cottrell, M. J. 1980, *AJ*, 85, 22, doi: [10.1086/112629](https://doi.org/10.1086/112629)
- Witt, A. N., Gordon, K. D., Vijh, U. P., et al. 2006, *ApJ*, 636, 303, doi: [10.1086/498052](https://doi.org/10.1086/498052)
- Witt, A. N., Petersohn, J. K., Bohlin, R. C., et al. 1992, *ApJL*, 395, L5, doi: [10.1086/186475](https://doi.org/10.1086/186475)
- Yasui, C., Kobayashi, N., Tokunaga, A. T., & Saito, M. 2014, *MNRAS*, 442, 2543, doi: [10.1093/mnras/stu1013](https://doi.org/10.1093/mnras/stu1013)
- Yoshikawa, T., Ikeda, Y., Fujishiro, N., et al. 2012, in *Society of Photo-Optical Instrumentation Engineers (SPIE) Conference Series*, Vol. 8444, *Ground-based and Airborne Telescopes IV*, ed. L. M. Stepp, R. Gilmozzi, & H. J. Hall, 84446G, doi: [10.1117/12.925428](https://doi.org/10.1117/12.925428)

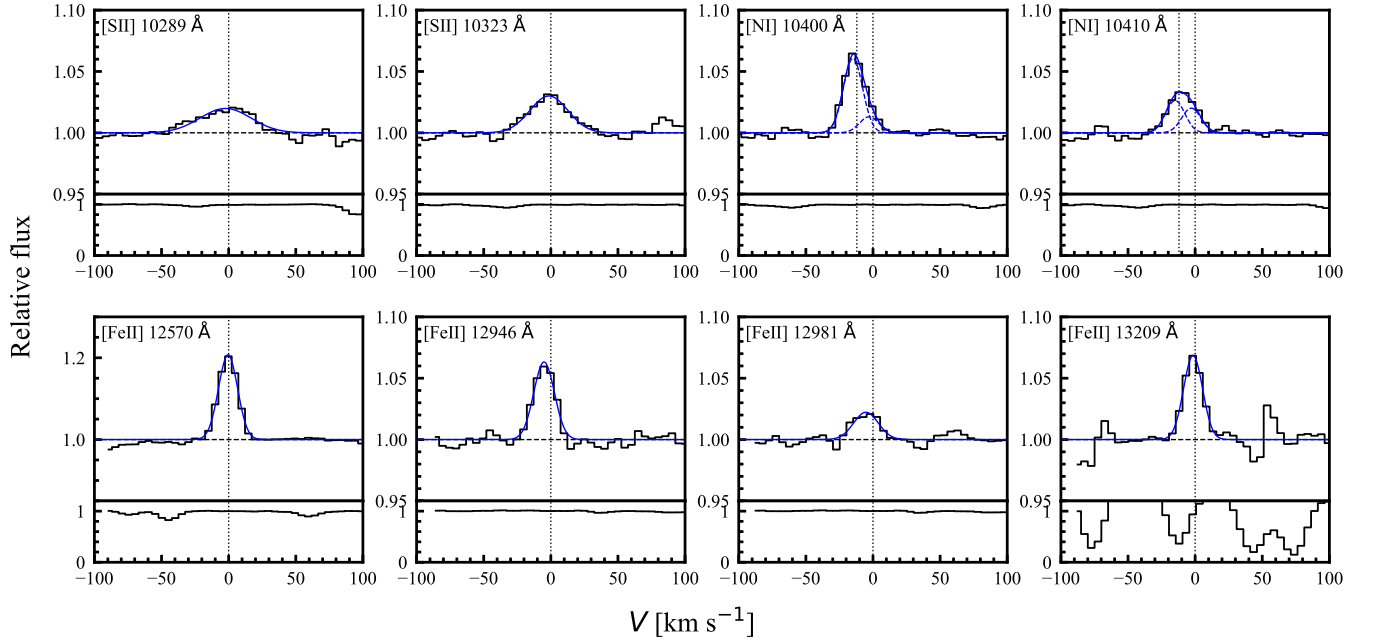
Table 1. Summary of WINERED Observations

Object	Spectral Type	Object Type	Obs Date (UT)	t_{exp}	Airmass
			(yyyy-mm-dd hh:mm-hh:mm)	(s)	(sec z)
HD 200775	B3	Target	2015-07-20 15:33-16:19	2400	1.2
ρ Peg	A1V	Telluric standard	2015-07-20 16:49-17:01	480	1.2

Table 2. Properties of Forbidden Lines Detected in HD 200775

Line	λ_{vac}	λ_{air}	A_{ul}	Transition	S/R	V_c	ΔV_{FWHM}	I_{peak}
	(\AA)	(\AA)	(s^{-1})			(km s^{-1})	(km s^{-1})	
(1)	(2)	(3)	(4)	(5)	(6)	(7)	(8)	(9)
[S II] 10289	10289.55	10286.73	1.15E-01	$3s^2 3p^3 \ ^2D_{3/2}^o - 3s^2 3p^3 \ ^2P_{3/2}^o$	12.5	-2.3 ± 2.3	43.2 ± 5.1	0.020 ± 0.002
[S II] 10323	10323.32	10320.49	1.57E-01	$3s^2 3p^3 \ ^2D_{5/2}^o - 3s^2 3p^3 \ ^2P_{3/2}^o$	20.8	-1.5 ± 1.7	31.3 ± 3.5	0.030 ± 0.003
[N I] 10400	10400.59	10397.74	6.10E-02	$2s^2 2p^3 \ ^2D_{5/2}^o - 2s^2 2p^3 \ ^2P_{1/2}^o$	45.6	-2.9 ± 1.1	12.3 ± 1.3	0.061 ± 0.003
	10401.00	10398.16	3.45E-02	$2s^2 2p^3 \ ^2D_{5/2}^o - 2s^2 2p^3 \ ^2P_{3/2}^o$				0.013 ± 0.002
[N I] 10410	10410.02	10407.16	2.64E-02	$2s^2 2p^3 \ ^2D_{3/2}^o - 2s^2 2p^3 \ ^2P_{3/2}^o$	17.3			0.026 ± 0.001
	10410.44	10407.59	5.31E-02	$2s^2 2p^3 \ ^2D_{3/2}^o - 2s^2 2p^3 \ ^2P_{1/2}^o$				0.020 ± 0.003
[Fe II] 12570	12570.21	12566.77	4.74E-03	$3d^6 \ (^5D) 4s a \ ^6D_{9/2} - 3d^6 \ (^5D) 4s a \ ^4D_{7/2}$	53.0	-0.5 ± 1.0	12.1 ± 0.8	0.207 ± 0.006
[Fe II] 12946	12946.20	12942.66	1.98E-03	$3d^6 \ (^5D) 4s a \ ^6D_{5/2} - 3d^6 \ (^5D) 4s a \ ^4D_{5/2}$	24.7	-5.0 ± 1.1	14.0 ± 1.3	0.063 ± 0.003
[Fe II] 12981	12981.25	12977.70	1.08E-03	$3d^6 \ (^5D) 4s a \ ^6D_{1/2} - 3d^6 \ (^5D) 4s a \ ^4D_{3/2}$	11.2	-5.2 ± 1.6	18.3 ± 3.3	0.022 ± 0.003
[Fe II] 13209	13209.11	13025.50	1.31E-03	$3d^6 \ (^5D) 4s a \ ^6D_{7/2} - 3d^6 \ (^5D) 4s a \ ^4D_{7/2}$	10.7	-1.5 ± 1.8	12.1 ± 4.9	0.069 ± 0.013

NOTE—Column (2): wavelength in a vacuum. Column (3): wavelength in the air. Column (4): Einstein A coefficient. Column (6): S/N. Column (7): centroid velocity. Column (8): velocity width in FWHM. Column (9): peak intensity relative to the continuum level.

**Figure 1.** Line profiles of the forbidden lines detected in HD 200775 (upper panels). The spectra obtained with WINERED are shown in black, and the fitting results with the Gaussian profile are shown in blue. For [N I] lines, because each line is a doublet line, the obtained spectrum is fitted with two components and shown by the blue dashed line, and the composite of the two components is shown by the blue solid line. The velocities are relative to the stellar rest velocities. The normalized spectra of the telluric standard star are shown in the lower panels.

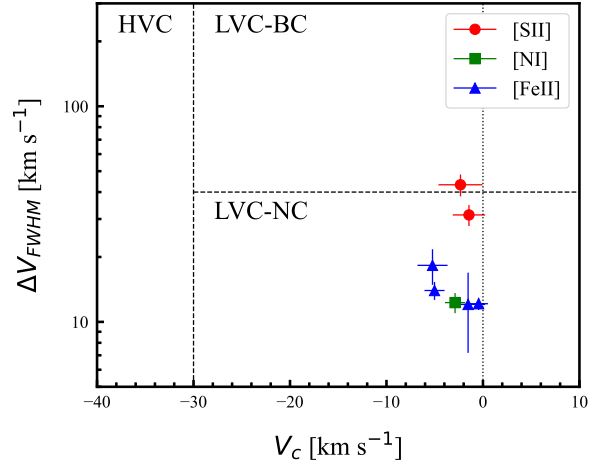


Figure 2. Velocity properties (V_c vs. ΔV_{FWHM}) of the detected forbidden lines in HD 200775. The circles, squares, and triangles with error bars show [S II], [N I], and [Fe II], respectively. The classifications divided by the dashed lines, HVC ($V_c \lesssim -30 \text{ km s}^{-1}$), LVC-BC ($V_c \gtrsim -30 \text{ km s}^{-1}$ and $\Delta V_{FWHM} \geq 40 \text{ km s}^{-1}$), and LVC-NC ($V_c \gtrsim -30 \text{ km s}^{-1}$ and $\Delta V_{FWHM} \leq 40 \text{ km s}^{-1}$), were adapted from [Simon et al. \(2016\)](#).

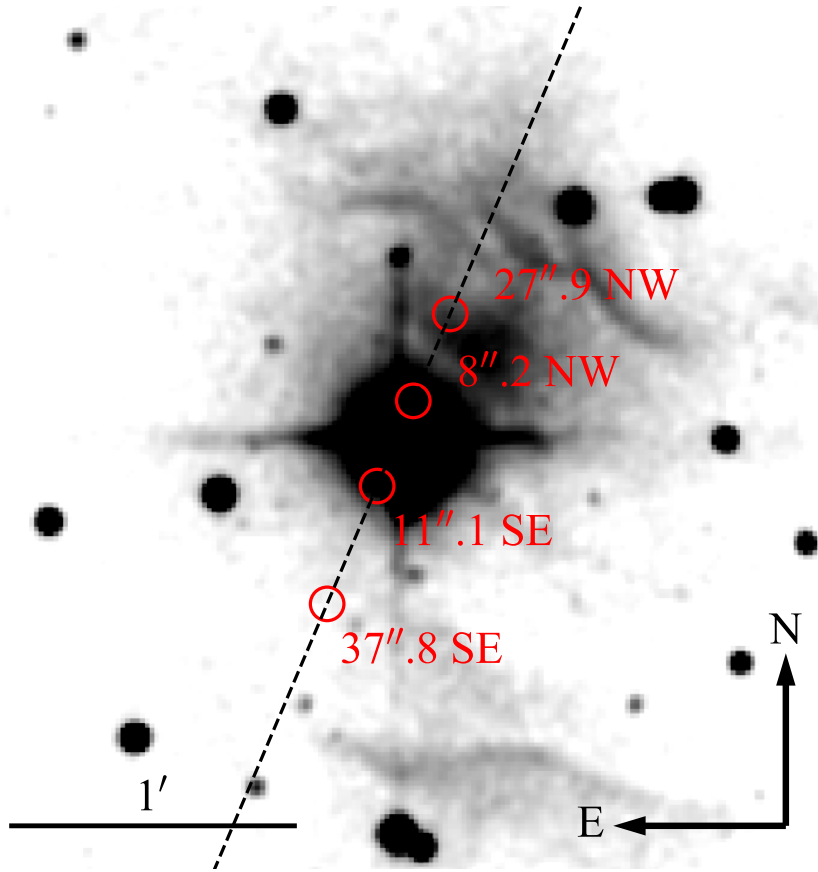


Figure 3. Spatial map around HD 200775. Red circles indicate the positions of the reference regions superposed on the Two Micron All Sky Survey J band image. The size of each circle is the seeing size.

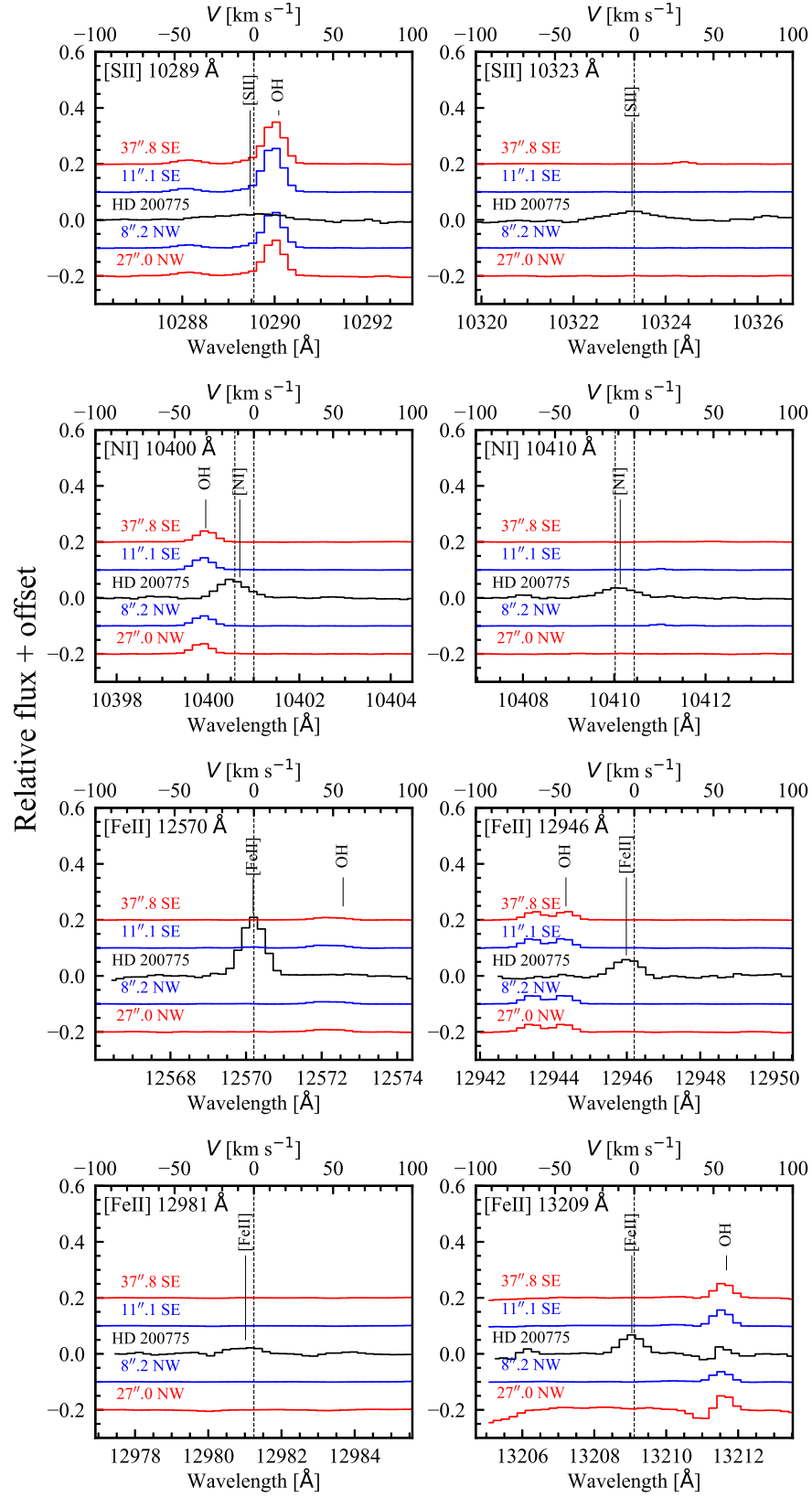


Figure 4. Spectra of reference regions, surrounding HD 200775, and around the wavelengths of the forbidden lines (colored lines). The intensities of the reference spectra are corrected to be comparable to the continuum line of HD 200775. For reference, the spectra of HD 200775 are shown by black lines. The locations of the detected forbidden lines are indicated by the respective line names. OH emission lines of terrestrial atmospheric origin (Oliva et al. 2013) are labeled “OH” in the figure.